Eur. Phys. J. D **16**, 249–252 (2001)

THE EUROPEAN PHYSICAL JOURNAL D

EDP Sciences

The effect of oxidation on the structure of nickel nanoparticles

B. Rellinghaus[1,a], S. Stappert[1], E.F. Wassermann[1], H. Sauer[2], and B. Spliethoff[3]

[1] Experimentelle Tieftemperaturphysik, Gerhard-Mercator Universität, D-47048 Duisburg, Germany
[2] Anorganische Chemie, Fritz-Haber-Institut der Max-Planck-Gesellschaft, D-14195 Berlin, Germany
[3] Abt. für Elektronenmikroskopie, Max-Planck-Institut für Kohleforschung, D-45479 Mülheim, Germany

Received 21 December 2000

Abstract. The structural properties of nickel nanoparticles which are prepared by means of DC sputtering in argon and subsequently oxidized in ambient air are reported. *Ex situ* structural and chemical investigations utilizing (high resolution) transmission electron microscopy and electron energy loss spectroscopy reveal that the particles consist of a metallic core surrounded by an oxide shell. The lattice constant of the nickel core is found to increase significantly with decreasing particle size. This widening of the nickel lattice is attributed to an interfacial stress that originates from the lattice mismatch between nickel and nickel oxide.

PACS. 61.46.+w Nanoscale materials: clusters, nanoparticles, nanotubes, and nanocrystals – 61.16.Bg Transmission, reflection and scanning electron microscopy

1 Introduction

In recent years, the size reduction of magnetic nanoparticles has gained tremendous interest in a variety of fields such as the attempt to increase the areal storage density of magnetic recording media [1] or the design of magnetic sensors. However, in order to make use of the properties of individual particles, effective control of the coupling between the magnetic entities is essential. The magnetic nanoparticles are therefore either coated with or embedded in a non-magnetic or antiferromagnetic material [2, 3]. Since the surface-to-volume ratio increases with decreasing particle size, the influence of the coating on the structure and properties of the core particle is of growing importance.

In the present work, we study the structure of gas-phase prepared nickel nanoparticles which are surrounded by a natural oxide shell. Particular attention is paid to the size-dependent influence of the oxide shell on the metallic nickel core.

2 Experimental

Nickel nanoparticles are prepared by means of a DC sputtering process in argon atmosphere. The details of the preparation process are described elsewhere [4]. During the particle preparation the sputtering power and argon pressure are varied in the ranges 100 W $\leq P_{\mathrm{DC}} \leq$ 250 W and 0.3 mbar $\leq p_{\mathrm{prep}} \leq$ 0.9 mbar, respectively. Particles are deposited onto amorphous carbon films which are supported by copper grids suitable for *ex situ* morphological, structural, and spectroscopic investigations by means of transmission electron microscopy (TEM). Particles which are deposited at a position immediately opposite to the sputter gun are referred to as "primary" particles. In addition, the particles can be subjected to a sintering process in the gas phase prior to their deposition ("sintered" particles). We emphasize that all samples are exposed to ambient air prior to any *ex situ* investigations.

For morphological investigations and structure determination *via* electron diffraction we use a Philips CM 12 (Twin) microscope with LaB_6 filament. High resolution TEM investigations (HRTEM) are carried out on a Hitachi HF 2000 and a Philips CM 200 FEG (Super Twin) microscope. The latter is also used to conduct electron energy loss spectroscopy (EELS) experiments on individual particles utilizing a Gatan Imaging Filter.

3 Results and discussion

Fig. 1 shows a background subtracted line scan across the electron diffraction pattern (EDP) of a sample containing nickel primary particles with a mean particle size of $d_{\mathrm{P}} = 4.1$ nm ($P_{\mathrm{DC}} = 250$ W, $p_{\mathrm{prep}} = 0.5$ mbar). From the occurrence of diffraction fringes in the EDP it is clear that the nanoparticles are crystalline. A comparison of the EDP with the position of the Bragg peaks for bulk fcc Ni (grey bars) shows that the deposited particles are predominantly Ni. However, as indicated by the shoulder at a radius of roughly $R \sim 15$ mm in the first peak and

[a] e-mail: brell@ttphysik.uni-duisburg.de

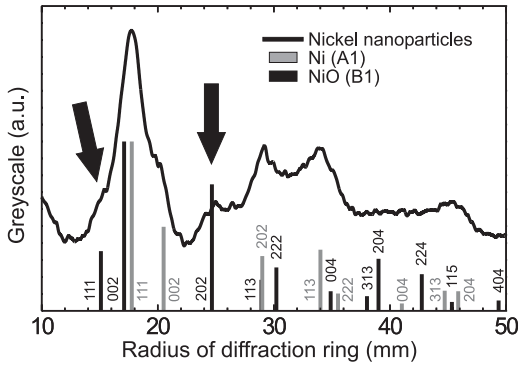

Fig. 1. Electron diffraction on nickel primary particles. The grey and black bars indicate the position and intensity of Bragg peaks for bulk Ni and NiO, respectively.

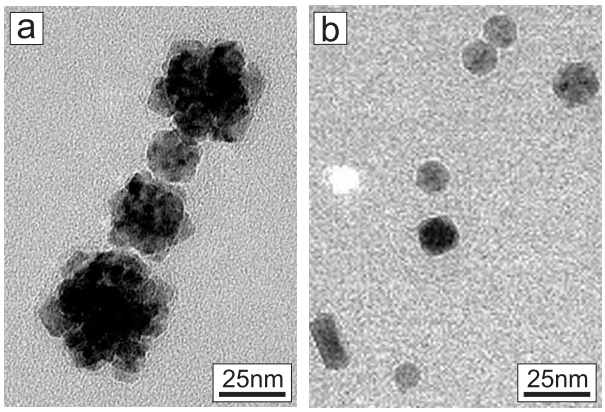

Fig. 2. TEM micrographs of sintered nickel nanoparticles deposited onto amorphous carbon films. (a) Poly-agglomerate particle. (b) Single predominantly multiply twinned particles.

a maximum at $R \sim 24.5$ mm (*cf.* black arrows in Fig. 1) which are in exact agreement with the positions of the (111) and (202) Bragg peaks of NiO, there are NiO phase contributions present in the sample.

When the nickel particles are sintered in the gas-phase at room temperature (RT) we obtain two classes of nanoparticles: Fig. 2a shows the TEM image of a large chain-like agglomerate that consists of four smaller poly-crystalline particles. We refer to particles of this type as "poly-agglomerates". In addition we observe the occurrence of smaller single particles which are strongly faceted (Fig. 2b). Detailed analysis by means of electron diffraction and HRTEM investigations reveals that these particles have a multiply twinned structure [5].

In order to study the oxidation process in more detail, RT-sintered Ni nanoparticles are deposited onto ultra-thin holey carbon films. In Fig. 3 we show the TEM micrograph of a poly-agglomerate that protrudes into a hole in the amorphous carbon film and is thus an ideal candidate for local EELS investigations. The white circles labeled A-D mark the areas where we have measured electron energy loss (EEL) spectra, and the results are shown in Fig. 4. The intensities obtained from the positions A-D are plotted as function of the loss energy in the vicinity of (a) the

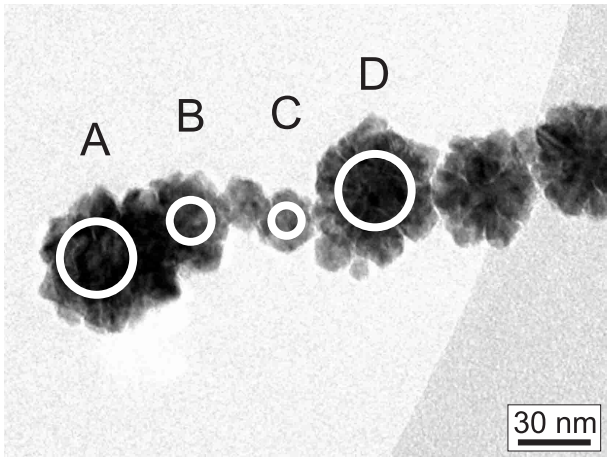

Fig. 3. TEM micrograph of a nickel poly-agglomerate deposited onto holey amorphous carbon film. The white circles labeled A-D indicate the areas where EEL spectra are taken.

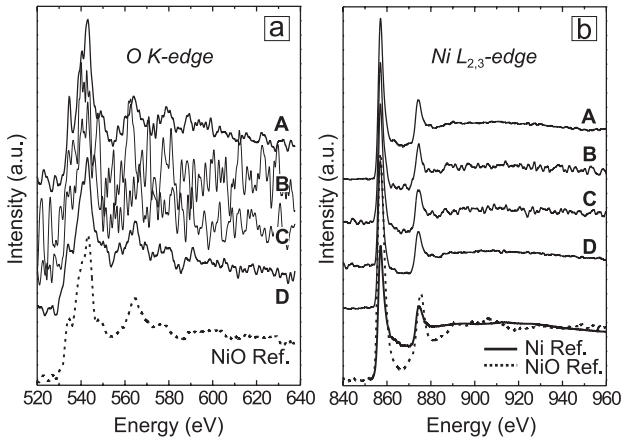

Fig. 4. EEL spectra obtained from the areas A-D of the particle shown in Fig. 3: (a) O K-edge and (b) Ni $L_{2,3}$-edge. The Ni edge is in good agreement with reference data for Ni [6], and the O edge is in accordance with the data for NiO [7].

O K-edge and (b) the Ni $L_{2,3}$-edge (data are separated from one another by arbitrary offsets). In case of the O K-edge (Fig. 4a) the spectra are in good agreement with the literature data on NiO (dotted line) [6]. Even for the results obtained from positions B and C, which are somewhat noisy due to the smallness of the measuring areas, this agreement with the reference data is obvious. From Fig. 4b on the other hand, we find that the EEL spectra in the vicinity of the Ni $L_{2,3}$-edge are comparable rather to what is expected for elemental Ni [7] than to the data for NiO [6]. It is thus to be concluded that the oxygen atoms are placed in a local environment of NiO, whereas the majority of the nickel atoms is surrounded by elemental Ni. This result is in accordance with the assumption that the final particles consist of a metallic Ni core surrounded by a passivating NiO shell.

In order to confirm this conclusion we study the recrystallization process of an individual particle under the

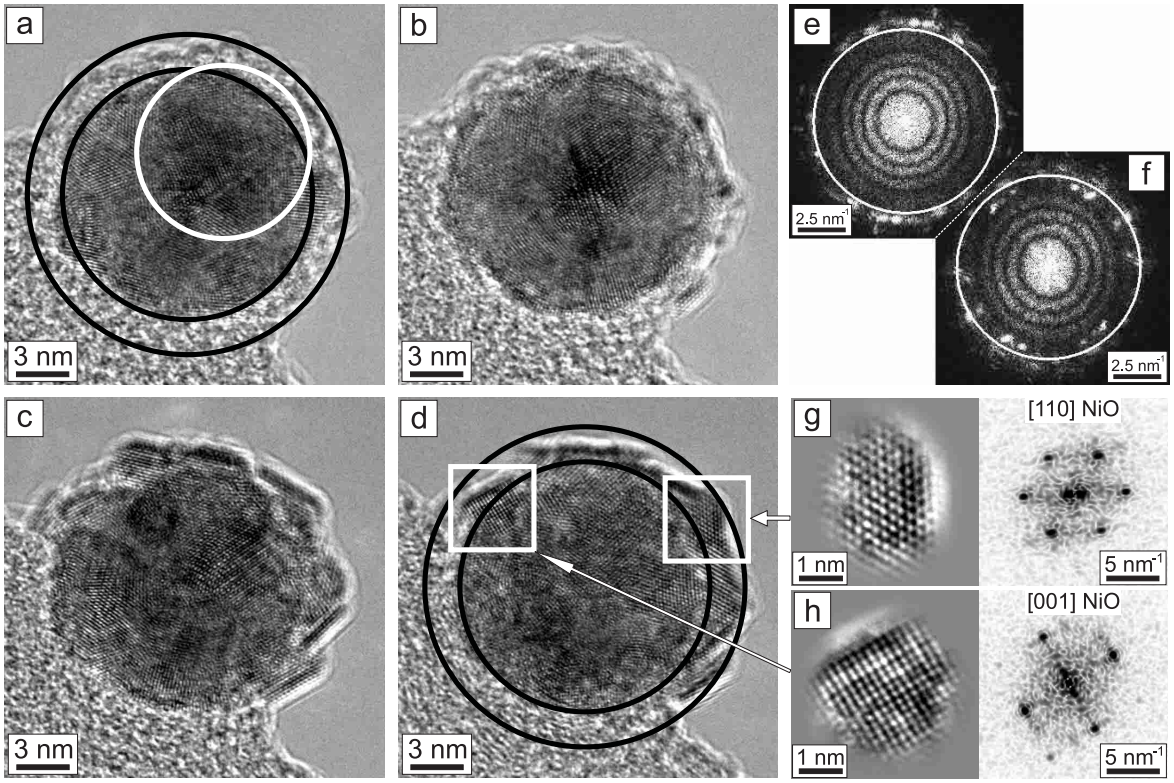

Fig. 5. Chronological series (a-d) of HRTEM images of a nickel nanoparticle on an amorphous carbon film. The particle shell is indicated by the area between two black circles in both, the initial (a) and the final state images (d). The white circle in (a) marks the area where an EEL spectrum has been taken. (e) and (f) show power spectra of the initial and the final state images, respectively. The white circles in the power spectra indicate radii of spatial frequencies of $\nu = 4.87$ nm^{-1}. (g) and (h) present magnified sections of (d) together with the corresponding power spectra. See text for details.

influence of the electron beam *in situ* in the TEM. In Fig. 5 we show a chronological series (a-d) of HRTEM images of a Ni particle that has been exposed to the beam for approximately half an hour in total. Figs. 5a and 5d show the particle at the beginning and the end of the investigation and we refer to them as the initial and final state images, respectively. The projected surface area of the particle marked by the area between the concentric black circles appears amorphous in the initial state image. As evidenced by local EELS measurements, there is *no* carbon present in this surface region of the particle. With increasing exposure time (*i.e.* from (a) to (d)) we observe re-crystallization processes which occur just in this surface area and which result in the formation of small single crystals. Figs. 5g and 5h show magnifications of the areas marked by the white squares in the final state image together their power spectra as obtained from Fourier transformations. By measuring the angles and spacing between the various lattice fringes and intensity maxima in the power spectra ($\equiv$ reciprocal lattice points) the crystals are unambiguously determined to be NiO (NaCl-type, B1) seen along the [110] and [001] zone axes. In Figs. 5e and 5f we show the power spectra of the complete initial and final stage images, respectively. The white circles have a radius that corresponds to a spatial frequency of $\nu = 4.87$ nm$^{-1} = 1/(0.205$ nm) and thus mark the maximum lattice spacings that is expected to occur for fcc Ni ($d_{\max}$(Ni) $= d_{111} = 0.2035$ nm). This means that any reciprocal lattice point that lies inside the circles belongs to a lattice spacing that is larger than what is expected to occur for elemental Ni. Whereas in Fig. 5e (initial state) all occurring spots lie outside the delimiting circle, the majority of the spots that are seen in Fig. 5f (final state) lies inside the circle. This finding thus confirms the result that the surface crystallites that are formed under the influence of the electron beam are NiO.

Fig. 6 shows (a) the O K-edge and (b) the Ni $L_{2,3}$-edge as obtained by EELS measurements in the initial state from the area indicated by the white circle in Fig. 5a. The Ni $L_{2,3}$-edge is again in good agreement with the reference spectrum for elemental Ni. For the O K-edge, we find some slight deviations from both, the reference data of NiO and the results obtained from the poly-agglomerate (*cf.* Fig. 4a). Although the signal is somewhat noisy it can be seen that the pre-peak at a loss energy of roughly 535 eV is less intense than in the reference spectrum for NiO. Also at higher energies, the experimental line profile does not resemble the double-peak structure (at ~ 565 eV and ~ 600 eV) of the reference. We assume that these discrepancies are due to the fact that at the beginning of the exposure to the electron beam, the oxidized surface of the particle is amorphous rather than crystalline.

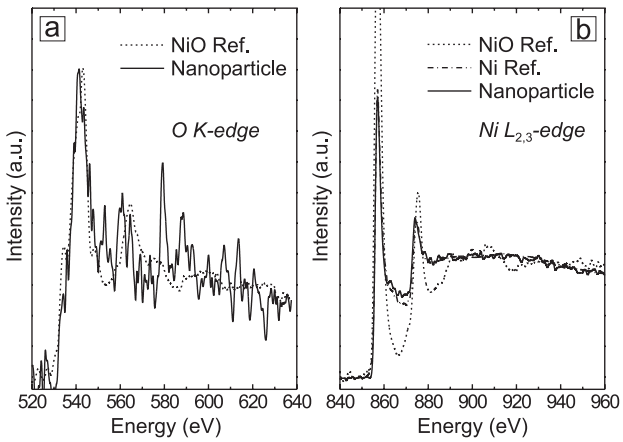

Fig. 6. EEL spectra of the particle shown in Fig. 5a (from the area within the white circle): (a) O K-edge, (b) Ni $L_{2,3}$-edge. Results are compared to reference data on Ni [6] and NiO [7].

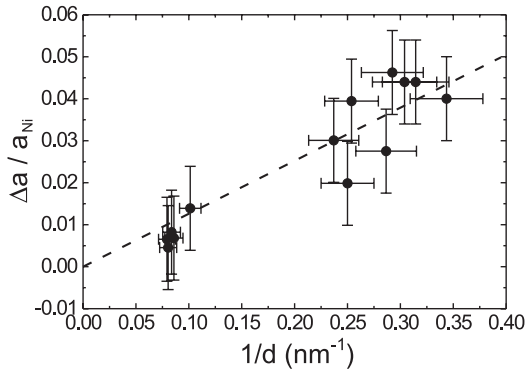

Fig. 7. Relative change of the lattice constant, $\Delta a/a_0$, as function of the reciprocal particle size, $1/d$.

Since the lattice constant of NiO ($a_{\mathrm{NiO}} = 0.4203$ nm) is larger than that of elemental Ni ($a_{\mathrm{Ni}} = 0.3524$ nm) [8], the assumption lies close that there is a size dependent relaxation of the lattice constant of the Ni core which stems from the interface stress between the metallic core and the oxidic shell [9]. We have therefore conducted electron diffraction experiments on a series of samples with both, primary and sintered particles. In Fig. 7 we plot the resulting relative change of the lattice constant of the Ni core, $\Delta a/a_{\mathrm{Ni}}$, as function of the reciprocal particle size, d. With decreasing d we observe an increase of the lattice constant of up to 4.5%. The dashed line in Fig. 7 represents a fit of the Laplace equation [9]

$$\frac{\Delta a}{a_{\mathrm{Ni}}} = -\frac{4 f \kappa_{\mathrm{Ni}}}{3d} \qquad (1)$$

to the experimental data. Here, f denotes the effective surface tension (*i.e.* the interface stress), and $\kappa_{\mathrm{Ni}} = 5.4 \times 10^{-12}\ \mathrm{m^2\,N^{-1}}$ is the compressibility of bulk Ni at RT [10]. As a result, we obtain $f = -17.5\ \mathrm{N\,m^{-1}}$, whereas in the case of pure Ni particles in vacuum, one would expect a small and positive surface tension of roughly $f_{\mathrm{Ni}} = +2.24\ \mathrm{N\,m^{-1}}$ [11]. In a simple model calculation, where we assume that the oxide shell consists of a monolayer of NiO(001) that is epitaxially grown onto a Ni(001) particle surface, we have estimated the effective surface tension due to the lattice mismatch between NiO and Ni to be $f^* = -14.8\ \mathrm{N\,m^{-1}}$ [12], which is comparable to our experimental result. However, the magnitude of f^* increases linearly with the number of oxide monolayers and may thus easily assume values that are by far larger than the experimental value. In some HRTEM investigations predominantly on cubic particles with (001)-facettes we find that individual NiO surface crystallites are indeed epitaxially related to the Ni core, and even a continuous widening of the lattice when going from Ni to NiO can be observed. However, the data presented in Fig. 7 are averages over ensembles of many nanoparticles each of which contributes to the measured lattice constant with its individually structured interface. As a consequence, the result of our estimation is to be regarded purely qualitative.

4 Summary

Ni nanoparticles which are prepared and sintered in the gas phase are oxidized in ambient air. (HR)TEM and EELS investigations show that the particles exhibit a distinct core-shell structure with a metallic Ni core surrounded by a passivating shell of NiO. The lattice mismatch between metal and oxide causes the formation of an interfacial stress that results in a successive widening of the Ni lattice with decreasing particle size.

References

1. D. Weller, A. Moser, L. Folks, M.E. Best, W. Lee, M.F. Toney, M. Schwickert, J.-U. Thiele, M.F. Doener, IEEE Trans. Mag. **36**, 10 (2000).
2. D.L. Peng, K. Sumiyama, T. Hihara, S. Yamamuro, T.J. Konno, Phys. Rev. B **61**, 3103 (2000).
3. S. Sun, C.B. Murray, D. Weller, L. Folks, A. Moser, Science **287**, 1989 (2000).
4. S. Stappert, B. Rellinghaus, Ch. Fell, H. Zähres, E.F. Wassermann, H. Sauer, B. Spliethoff, to be published.
5. S. Stappert, Ch. Fell, H. Zähres, B. Rellinghaus, E.F. Wassermann, H. Sauer, *Proc. of the 12th Europ. Congress on Electron Microscopy EUREM 12* (2000), Vol. II, pp. 373-374.
6. R.D. Leapman, L.A. Grunes, P.L. Fejes, Phys. Rev. B **26**, 614 (1982).
7. O.L. Krivanek, C.C. Ahn, *Gatan EELS Atlas.*
8. W.B. Pearson, *Handbook of Lattice Spacings and Structures of Metals and Alloys* (Pergamon Press, New York, 1958).
9. H. Hofmeister, F. Huisken, B. Kohn, Eur. Phys. J. D **9**, 137 (1999).
10. F. Kohlrausch, *Praktische Physik* (B.G. Teubner, Stuttgart, 1968).
11. J. Wan, Y.L. Fan, D.W. Gong, S.G. Shen, X.Q. Fan, Modelling Simul. Mater. Sci. Eng. **7**, 189 (1999).
12. S. Stappert, Diploma thesis, Gerhard-Mercator University, Duisburg, Germany, 2000.